ELSEVIER

Comput. Methods Appl. Mech. Engrg. 190 (2001) 6053–6073

Computer methods in applied mechanics and engineering

www.elsevier.com/locate/cma

Incipient sliding of rough surfaces in contact: a multiscale numerical analysis

M. Borri-Brunetto [a], B. Chiaia [a,*], M. Ciavarella [b]

[a] *Department of Structural and Geotechnical Engineering, Politecnico di Torino, Corso Duca degli Abruzzi 24, 10129 Torino, Italy*
[b] *CNR – I.R.I.S. – Computational Mechanics of Solids, Str. Crocefisso 2/B, 70126 Bari, Italy*

Received 30 May 2000

Abstract

In this paper, the Cattaneo theory of frictional contact is extended to elastic half-spaces in contact through rough disordered interfaces. The discrete version of the Cattaneo theorem is provided, and represents the basis of a multiscale numerical contact algorithm. Mathematical surfaces with imposed roughness, as well as experimentally digitised ones, are analysed. By means of a numerical method, the evolution of the contact domain, at different resolution, is investigated. Roughness of the interfaces provides lacunarity of the contact domains, whose fractal dimension is always smaller than 2.0. When a tangential force is applied, the extent of the stick area decreases in the same way as the contact area develops with increasing pressure, and the slip area is found to be proportional to the tangential force, as predicted by Cattaneo theory. The evolution of the shear centroid, as well as the amount of dissipated energy up to full-sliding, are provided. Finally, it is shown that, at a sufficient level of discretization, the distribution of contact pressures is multifractal.

1. Introduction

1.1. Cattaneo's approach to tangential contact

Contact mechanics has occupied a central place in the development of several areas of research, like tribology, solid mechanics, machine design but also geology, study of earthquakes and other fields. The paper by Hertz [1] gave the solution for the frictionless normal contact of two elastic bodies of quadratic profile, and consequently the basis for design procedures used nowadays in many industrial situations involving elastic contact. The subject has since then seen considerable development, both from a mathematical standpoint, and from that proper of engineers, as the monograph by Johnson [2] illustrates in its excellent overview.

A contact problem involves the determination of the traction distributions transmitted from one surface to the other, in general involving normal pressures and, if friction is present, shear tractions, according to an appropriate set of equalities and inequalities governing the physics of the contact. When there is friction at the contact interface, 'Coulomb' friction behaviour is usually introduced to give the conditions necessary to determine the shear traction distribution: any point in the contact area must be either in *stick*, or *slip*, and the tangential tractions must behave accordingly. Frictional slip is essentially an incremental process and hence the solution depends on the history of loading, even if the loading rate is slow enough to define a *quasi-static* solution, which is what we will assume in the following.

* Corresponding author. Tel.: +39-11-564-4866; fax: +39-11-564-4899.
E-mail address: chiaia@polito.it (B. Chiaia).

0045-7825/01/$ - see front matter
PII: S0045-7825(01)00218-3

The first contact problem transmitting tangential forces was solved by Cattaneo [3], who considered the extension of the Hertz problem (between similar materials) with a monotonically increasing tangential force at constant normal pressure. Similar results were obtained, apparently in an independent manner, by Mindlin [4]. In this problem, slip occurs in an elliptical annulus homothetic to the contact area, starting from the edges of it – that is to say the points at lower pressure are the first to slide – and the resulting shear traction distribution is the difference between the traction distribution at limiting friction and an opposing distribution in the central ellipse. Cattaneo's results were extended to other loading scenarios by Mindlin and Deresiewicz [5]. A significant generalization of these results has recently been discovered by Ciavarella [6], who showed that the frictional traction distribution satisfying both equality and inequality conditions for *any* plane contact problem (not necessarily Hertzian) will consist of a superposition of the limiting friction distribution and an opposing distribution equal to the coefficient of friction multiplied by the normal contact pressure distribution at some smaller value of the normal load. Thus, as the tangential force is increased at constant normal force, the stick zone shrinks, passing monotonically through the same sequence of areas as the normal contact area passed through during the normal loading process. Jäger [7] established results similar to those of [6], for more general loading scenarios.

The Cattaneo solution, valid for plane contact, can be in principle extended to the general three-dimensional contact problem only when the Poisson's ratio is zero. In all other cases, the Cattaneo's traction distribution satisfies the limiting friction equations but predicts a mismatch between the direction of the traction and the direction of slip. However, similar conditions apply to the original Cattaneo and Mindlin solutions and the effects of this error have been shown to be small in particular cases. With this caveat, the solution can probably be automatically extended to the general loading case using the arguments of Jäger [7]). [1]

1.2. Role of surface roughness

Most of the classical solutions of contact problems, starting from the Hertzian case, rely on the assumption of nominally smooth geometries, which is reasonable at large enough scales. However, real surfaces are rough on the microscopic scale and the effect of roughness is important for a series of phenomena involving friction and wear. In contact mechanics, most models consider real surfaces as statistical distributions of asperities of prescribed shape, each of which can be more or less deformed, depending on its initial height and on the load distribution.

Early breakthrough in this area were made by Archard [12] and Greenwood and Williamson [13]. The first suggested a deterministic model of rough surfaces that is very prescient. Indeed, his construction of a cascade of smaller hemispherical asperities superposed on a larger scale, is what in the limit we would now call a "fractal" surface [14]. Greenwood and Williamson [13], on the other hand, considered statistical distributions of asperity heights, and discovered that the relations between load (or thermal and electrical conductivity) and total contact area are all linear, independently of the details of the local asperity behaviour. Archard had reached similar conclusions with his multiscale deterministic model, suggesting that these linear behaviours are a strong characteristics of rough contacts, as confirmed by the experimental observations and by the Amontons–Coulomb's law of friction in particular.

With modern experimental methods, measurements performed on fracture surfaces have revealed the existence of a hierarchy of scales up to the limits of experimental discrimination, and therefore attention is now focused to develop multiscale models reproducing most features of a real surface, whereas asperity model theories are being abandoned, because the definition of an asperity is scale dependent, as most of the quantities obtained from these models (like the mean and variance of the surface elevations, of the slopes and of the curvatures).

[1] Other results are known for twisting problems, i.e., where the remote displacement is torsional [8–11] in Hertzian contacts; however, even in the case of pure twist of Hertzian contacts, the equations become quite cumbersome, in particular in the case of elliptical contact [9], and therefore we do not address this configuration. In the case of general combination of remote rigid translation and rotation, this shear traction distribution follows a complex stick-slip patterns, and a fully numerical solution is necessary.

The linear relationships discussed above are very easily obtained with many models and coarse resolutions, but they are not the only feature to be extracted from a contact model. For example, the relationship between the total actual area of contact S and the normal load P is predicted to be almost linear, say $S = cP$, at all length scales, but the constant of proportionality c decreases with increasing resolution.

These multiscale effects indicate that a fractal description of the surface and of the contact process would be more appropriate [15]. Experimental spectral densities of the heights, $f(\omega)$, typically show a power-law form $f(\omega) \sim \omega^{-\beta}$ at high frequencies ω, with an attenuation at low frequencies, associated with the finite length of the body. The fractal properties of rough surfaces can also be revealed by plotting various statistical measures of the profile on a logarithmic scale, in which case a true fractal will plot as a straight line, where the slope is linked to Δ, the *fractal dimension*, and the position of the line is linked to a constant related to the amplitude of the roughness. Typical rough surfaces are found to lie in the range $2.0 < \Delta < 2.5$ [16]. The advantage of the fractal description is that it eliminates the implied truncation at small length scales by assuming that the same power-law behaviour continues without limit. In the same way, the spectral density of the heights is assumed to maintain the same power-law form for arbitrarily large ω.

Majumdar et al. [15,17] argued, for a plane contact of fractal surfaces (using Weierstrass-type functions), that the distribution of actual contact area sizes would follow power-law behaviour, based on geometrical considerations on the distribution of "islands" generated by cutting the surface at a constant height z. Neither attention was paid to the effect of elastic deformation on the distribution of contact areas, nor to elastic interaction among the asperities. A direct treatment of a fractal normal contact problem, fully taking into account elastic deformations of the half-spaces, has been proposed by Borri-Brunetto et al. [18]. A few large actual areas of contact are obtained at coarse grids. As the grid is refined, these break up progressively into clusters of smaller and smaller areas and the total area of actual contact decreases. This suggests that, in the fractal limit, the contact consists of an infinite number of infinitesimal contact points of zero total area, in agreement with Archard's results. In the particular case of a two-dimensional Weierstrass profile, this assumption has been mathematically proved [19].

In this paper, the discrete version of the Cattaneo–Mindlin theorem for rough surfaces is put forward. First, the equations of pointwise elastic contact are outlined. The solution is then implemented into a multiscale numerical method able to solve the normal and tangential contact problem at any resolution. The algorithm is applied to synthetic fractal surfaces and to a real rock fracture surface. The mechanical response, as well as the characteristics of the contact domains, are investigated. The solution for tangential loadings permits to follow the partial-slip regime and calculate, at any stage, the position of the centroid of shear tractions and the amount of dissipated energy. The distribution of contact micro-forces is eventually shown to be multifractal. Moreover, the width of the multifractal spectra increases with load, as the range of the stress singularities increases.

2. Discrete normal contact of rough surfaces

We shall focus on the problem of an imposed tangential shift with fixed normal load. Notice that in normal contact case the half-spaces may have different elastic properties if the contact is *frictionless*. In the case of tangential loading, this implies a trivial solution, so will not be considered. On the other hand, the *coupled* problem, making use of the full Green's function, is of cumbersome solution even in the simplest loading and geometrical cases already with only normal load [2]. Notice that, as we shall be dealing with the case of isotropic materials, elastic similarity is ensured when β, the second Dundurs' constant, is zero. For this case, we do not need all the terms in the Green's function, and normal and tangential problems are uncoupled [20].

In general, there is coupling between tangential and normal displacements, and therefore between pressures and shear tractions. Let us write the *elastic* surface displacements relative to the undeformed condition as $\mathbf{u}_1 = \{u_{x1}, u_{y1}, u_{z1}\}^{\mathrm{T}}$ and $\mathbf{u}_2 = \{u_{x2}, u_{y2}, u_{z2}\}^{\mathrm{T}}$. The relative displacement between two initially facing points is given by $\mathbf{u} = \mathbf{u}_1 - \mathbf{u}_2$, where the subscripts 1 and 2 indicate body 1 and 2, respectively. For the most general case of contact problem between half-spaces exchanging a set of concentrated forces

(tangential forces q_x, q_y and normal force p), the elastic displacements of the points at one surface are given by

$$u_{zi} = \frac{A}{2\pi}\sum_{j}^{N}\left[\frac{p_j}{r_{ij}} - \beta\left(\frac{(x_j - x_i)}{r_{ij}^2}q_{xj} + \frac{(y_j - y_i)}{r_{ij}^2}q_{yj}\right)\right], \tag{1}$$

$$u_{xi} = \frac{A}{2\pi}\sum_{j}^{N}\left[\frac{q_{xj}}{r_{ij}} - \beta\frac{(x_j - x_i)}{r_{ij}^2}p_j + \gamma\left(\frac{(x_j - x_i)^2}{r_{ij}^3}q_{xj} - \frac{(x_j - x_i)(y_j - y_i)}{r_{ij}^3}q_{yj}\right)\right], \tag{2}$$

$$u_{yi} = \frac{A}{2\pi}\sum_{j}^{N}\left[\frac{q_{yj}}{r_{ij}} - \beta\frac{(y_j - y_i)}{r_{ij}^2}p_j + \gamma\left(\frac{(y_j - y_i)^2}{r_{ij}^3}q_{yj} - \frac{(x_j - x_i)(y_j - y_i)}{r_{ij}^3}q_{xj}\right)\right], \tag{3}$$

where the sum is extended to all N contact points belonging to the contact domain S, as yet undetermined, r_{ij} is the distance between the point j where the force is applied and the point i where the displacement is measured, and A and γ are respectively the *composite compliance* and the *composite Poisson ratio* of the bodies [2]

$$A = \frac{1 - \nu_1}{\mu_1} + \frac{1 - \nu_2}{\mu_2}, \tag{4a}$$

$$\gamma = \left(\frac{\nu_1}{\mu_1} + \frac{\nu_2}{\mu_2}\right)\Big/A, \tag{4b}$$

where ν_i, μ_i are respectively the Poisson's ratio and the shear modulus of the material of the body i. In the general case, as formulated in Eqs. (1)–(3), exact analytical solutions are not known even in the simplest geometrical and loading configurations. However, the effect of coupling is generally small [21], and indeed there is a wide class of situations where the contacting bodies are of the same material, or the materials are elastically similar: more specifically, the case, where Dundurs' constant β is zero

$$\beta = \frac{\mu_2(\kappa_1 - 1) - \mu_1(\kappa_2 - 1)}{\mu_2(\kappa_1 + 1) + \mu_1(\kappa_2 + 1)} = 0, \tag{5}$$

where κ is the Kolosov's constant, given by $\kappa = (3 - 4\nu)$. In this case, the equations relating normal and tangential tractions become uncoupled, and the normal contact problem is independent of the tangential one. Then, the equation relating normal displacements to the pressure becomes, simplifying Eq. (1)

$$u_{zi} = \frac{A}{2\pi}\sum_{j}^{N}\left[\frac{p_j}{r_{ij}}\right]. \tag{6}$$

This discretized integral equation is sufficient to solve the normal contact problem, by imposing the appropriate boundary conditions. In particular, the equality (resp. inequality) relating to contact over the area S (resp. non-interpenetration condition exterior to S), are

$$u_{zi} = \delta_z - [\theta_x y_i + \theta_y x_i] - [h_1(x_i, y_i) - h_2(x_i, y_i)], \quad (x_i, y_i) \in S, \tag{7a}$$

$$u_{zi} > \delta_z - [\theta_x y_i + \theta_y x_i] - [h_1(x_i, y_i) - h_2(x_i, y_i)], \quad (x_i, y_i) \notin S, \tag{7b}$$

where $h_1(x, y)$, $h_2(x, y)$ are the functions describing the rough surfaces of the contacting bodies in the undeformed configuration, i.e., the elevations above a common datum; $(\delta_z, \theta_x, \theta_y)$ is the *relative* rigid body motion that brings the two bodies into contact. [3] Given $(\delta_z, \theta_x, \theta_y)$, the distribution of pressure $p(x, y)$ is

[2] Notice that A corresponds to $2/E^*$ in Johnson's notation [2].

[3] Note that, with the term *relative* displacement we intend the difference between the motion (elastic and/or rigid) of two points initially corresponding in the two bodies. Instead, with the term *elastic* displacement, we intend the displacements related to the purely elastic deformation of each body.

determined and, as a consequence, it is possible to compute a resultant load P and a resultant moment M of components M_x and M_y

$$P = \sum_j^N p_j, \quad M_x = \sum_j^N p_j y_j, \quad M_y = \sum_j^N p_j x_j. \tag{8}$$

The point where P can be applied without any moment is called the *centroid* of the normal pressure distribution, and is indicated by G_P.

3. Multiscale analysis and results of the normal contact problem

3.1. Numerical procedure

Since analytical solutions can be obtained only to a very limited category of problems, there has been considerable development of numerical methods, as discussed in [22–26]. Contact algorithms are also routinely included in most commercial finite element packages. The unilateral contact problem has been extensively approached by many authors, often as a non-linear optimization problem [22]. In our case, an incremental active set strategy has been preferred. The algorithm has been designed to determine the geometrical properties of the contact domain S between two linear-elastic half-spaces with a rough interface. In particular, we focus on the consequences of varying the *resolution* in the representation of the interfaces undergoing contact.

A discrete version of the problem is considered, by introducing in the reference plane x–y a square grid of points with spacing s. Of course, s is the scale chosen for solving the problem and corresponds to the resolution adopted in generating the mathematical surfaces or in digitizing the natural surfaces. At each node of the grid two material points can touch and transmit a force. We assume that a small contact zone is involved around the grid point. This contact region is supposed to be an indivisible *atom* of surface, whose area is related to the spacing s of the grid. This assumption, which is physically correct (since any measurement is performed at a given resolution), permits to avoid the point forces singularities.

Let δ_z be the relative displacement between two points far from the interface, assumed as positive in the closure direction. The function $\Delta h(x,y)$ – the *composite topography* – can be introduced, representing the *difference* between the maximum gap and the current gap of two corresponding points in the undeformed condition. It is well-known that, in normal elastic contact, $\Delta h(x,y)$ governs the mechanical response. In particular, due to the additivity of the power spectral densities of fractal surfaces, the problem of normal contact between two self-affine surfaces with given fractal dimensions can be transformed into the problem of the contact between the composite topography and a plane. The following linear system of equations can be written (in the simple case of two bodies with the same elastic properties)

$$\frac{-\delta_z + \Delta h_r}{2} = \sum_s H_{rs}\bar{p}_s \quad \forall P_r \in S, \tag{9}$$

where $\bar{p}_s$ is the resultant of the normal forces acting on the contact spot around point P_s and S is the set of the points undergoing true contact. The left-hand side of Eq. (9) has to be understood as a known imposed displacement $\hat{u}_z$. Note that the point force formulation (Eq. (6)) is not used directly, but is integrated over a circular area of radius $a = s/2$, as requested by the resolution adopted in the simulation. The influence terms H_{rs} are thus evaluated by referring to the settlements induced by a unit load applied to an elastic half-space through a rigid plate acting at point P_s

$$H_{rs} = \frac{1-\nu}{2\pi\mu a}\arcsin(a/r_{rs}), \tag{10}$$

where r_{rs} is the distance between P_r and P_s. By solving the system of Eq. (9), the contact forces between the two bodies are determined, provided the contact domain S is known. The solution is sought in terms of pressure and surface displacements, paying attention to the unilateral condition at the interface. This is

conveniently achieved by means of an incremental-iterative algorithm (*active set strategy*). In matrix form, the problem, at increment I, can be written as

$$\hat{\mathbf{u}}_I = \mathbf{H}_I \mathbf{p}_I, \tag{11}$$

where $\hat{\mathbf{u}}_I = \{u_{z1}, u_{z2}, \ldots, u_{zn}\}^{\mathrm{T}}$ is the n-component vector of the displacements imposed to the points of the current contact domain $S_I = (P_1, P_2, \ldots, P_n)$ for a given closure δ_{zI}, $\bar{\mathbf{p}}_I = \{\bar{p}_1, \bar{p}_2, \ldots, \bar{p}_n\}^{\mathrm{T}}$ is the vector of the unknown contact forces and $\mathbf{H}_I$ is the flexibility matrix.

The flexibility matrix $\mathbf{H}_I^{(1)}$ is assembled by adding, at each displacement increment I, the terms pertaining to the tentative domain $S_I^{(1)}$. The initial domain $S_I^{(1)}$ is chosen as the set that contains all those gridpoints which would compenetrate if contact forces were absent. Thereby, the normal contact forces $\mathbf{p}_I^{(1)}$ are evaluated. The points where tension forces are found, are eliminated from the contact domain, obtaining the new contact domain $S_I^{(2)}$ and the new matrix $\mathbf{H}_I^{(2)}$. After a few steps of the algorithm, through successive eliminations of tension points, the correct solution is attained for the displacement increment I. Then, the closure $\delta_{z(I+1)}$ is imposed, passing to a new increment. The solution of the simultaneous Eq. (11) is achieved with an iterative Gauss–Seidel method, taking into account the symmetry of matrix $\mathbf{H}_I$.

3.2. Multiscale analysis and lacunarity of the contact domains

When the evolutive contact problem is solved for a given interface, with a fixed fractal dimension Δ, but at different values of discretization s, the resulting contact domains S_s can be compared (Fig. 1). It can be easily realized that the concept of area of true contact [13], although representing a step forward with respect to the concept of apparent (nominally flat) area, is not able to describe consistently (that is, in a scale-independent manner) the interface interactions. As it clearly emerges from Fig. 1, the real contact area A_r progressively decreases with increasing the resolution of the discretization, ideally tending to zero in the theoretical limit of $s \to 0$.

This behaviour implies the lacunarity of the contact domain S, and therefore the necessity of abandoning the euclidean description and moving to the fractal model, characterized by the non-integer dimension Δ_σ ($\Delta_\sigma \leqslant 2.0$) of the domain S. This suggests that larger contact domains (i.e., larger apparent areas A_0) are less dense in the euclidean sense, that is, the probability of the occurrence of large zones without contact increases with the size of the interface. Application of the *box-counting method* [14] to a large number of contact sets (Fig. 2) allows to compute their Hausdorff dimension Δ_σ [18]. In this way, it is possible to compare the topology of the contact domains obtained for surfaces with different fractal dimensions and to follow the evolution of Δ_σ, for a given fractal surface, during the loading process. It is worth noting here that the contact domains are, to a great extent, self-similar sets, that is, they show isotropic scaling.

Following [27], let us consider now the following renormalization group:

$$P = \sigma_0 A_0 = \sigma_1 A_1 = \sigma_2 A_2 = \cdots = \sigma_n A_n = \cdots = \sigma^* \mathscr{H}_s, \tag{12}$$

where P is the applied normal load (scale-invariant quantity), A_n and σ_n are respectively the real contact area ($[\mathrm{L}]^2$) and the real mean pressure ($[\mathrm{F}][\mathrm{L}]^{-2}$) measured at the pre-fractal scale n, A_0 is the apparent

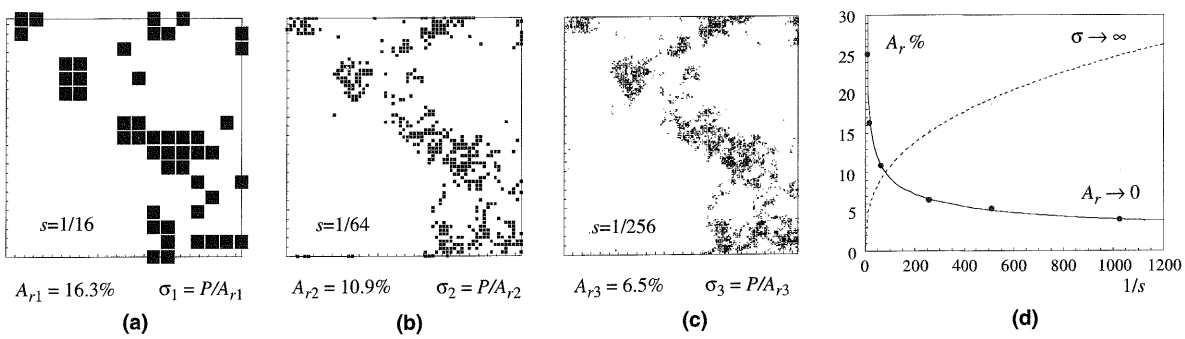

Fig. 1. Decrease of the real contact area and increase of the corresponding pressure (under the same external load) with increasing resolution ($\Delta = 2.1$, $\Delta_\sigma = 1.39$) (a)–(c), and power-law decrease of A_r (d).

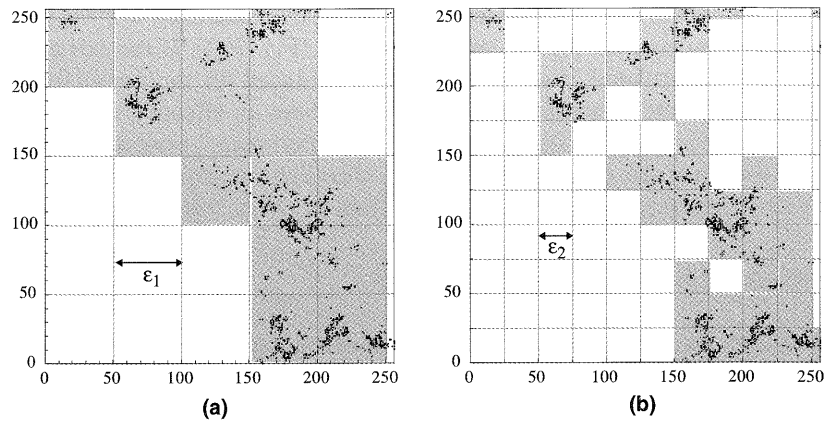

Fig. 2. Box-counting method applied to the contact domain generated by a Brownian surface ($\Delta = 2.5$) pushing against a flat half-space.

(nominally flat) area and $\sigma_0 = P/A_0$ is the apparent mean pressure. As one can realize from Fig. 1, at any given value of the normal load P, σ_n increases with increasing resolution and tends to infinity as $s \to 0$, because the euclidean measure ($[L]^2$) of the contact domain S vanishes. Hence, in the limit of the highest resolution, the classical definition of area (according to Lebesgue) loses its significance and leaves place to the *Hausdorff measure* $\mathscr{H}_S$ of the domain S (which is univocally defined by the non-integer dimensionality $[L]^{\Delta\sigma}$). Correspondingly, the *fractal mean pressure* σ^* can be defined as the dimensionally anomalous pressure acting at the fractal interface. Due to dimensional homogeneity, this quantity holds the physical dimensions $[F][L]^{-\Delta\sigma}$. By equating the second and the last term in Eq. (12) and taking the logarithm of both sides, if b is a characteristic linear size of the interface, the following scaling law is provided:

$$\log \sigma_0 = \log \sigma^* - (2 - \Delta_\sigma) \log b. \tag{13}$$

The fractal mean pressure σ^* represents the dominant quantity in the description of fractal contact. Two interfaces exchanging the same value of σ^* are assumed to behave similarly. Therefore, in order to achieve

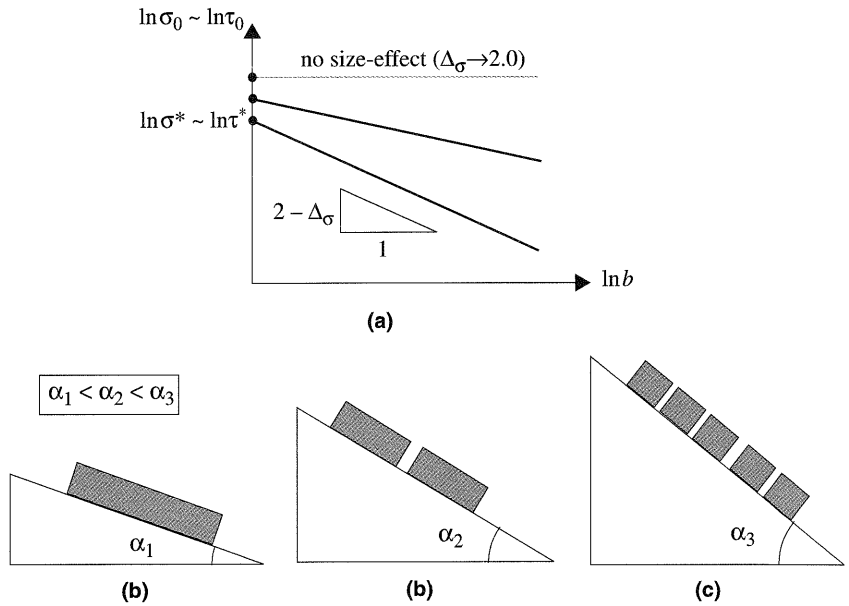

Fig. 3. Size-scale effects on the nominal pressure (and on the nominal shear strength) for different lacunarities Δ_σ corresponding to different fractal mean pressures σ^* (a). Schematic view of the size-scale effect on the limit slope angle (at constant apparent pressure) (b)–(d).

the same mechanical behaviour, the apparent macroscopic mean pressure $\sigma_0 = P/A_0$ must scale according to Eq. (13), stating its dependence on the size of the specimen (Fig. 3(a)). If the existence of a fractal limit shear traction $\tau^* = f^*\sigma^*$ is postulated, a scaling law can be deduced for the nominal friction coefficient f, i.e., $f = f^* b^{\lambda}$. Depending on the dimension of the domain where an effective shear strength can be activated, f may decrease with size (i.e., $\lambda < 0$), according to the experimental evidence of decreasing limit slope angle with increasing specimen size (Fig. 3(b)). This may shed light on many rock slope instabilities, which are not explicable when compared to the relatively high friction values measured on smaller specimens [28].

3.3. Mechanical response of mathematical fractal surfaces

Numerical simulations have been carried out by means of mathematical surfaces, generated by the *random midpoint displacement* (with fractal dimension Δ varying between 2.1 and 2.5), pushing against a flat

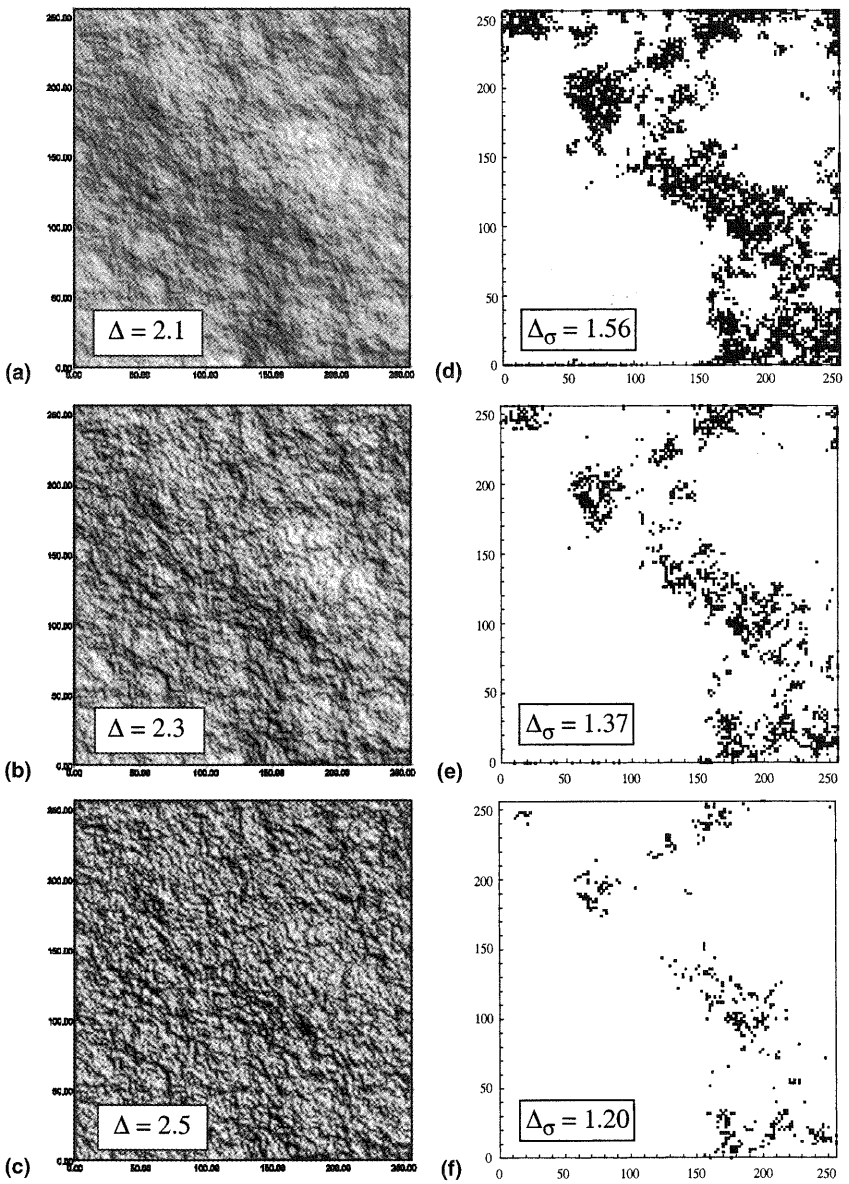

Fig. 4. Fractional Brownian surfaces generated by the random midpoint displacement method (a)–(c) and corresponding contact domains (d)–(f) at the same closure displacement.

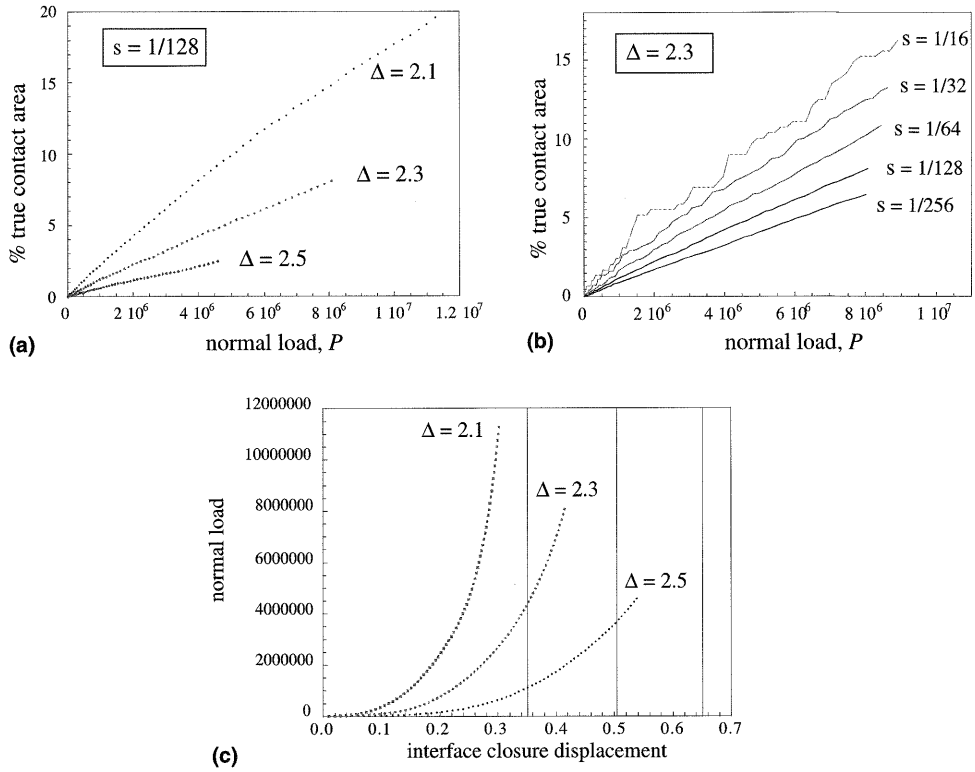

Fig. 5. Diagrams of the true contact area vs normal load for different fractal dimensions (at fixed resolution, (a)), and for different resolutions (at fixed fractal dimension, (b)). Computed normal load-joint closure laws and asymptotic values for different fractal dimensions (c).

plane. All the geometrical and mechanical parameters (e.g., Young's modulus, Poisson ratio, shape of the interface) have been kept the same in all the simulations. The contact domains obtained under the same value of the relative closure displacement δ_z, for three different values of the fractal dimension of synthetic contact surfaces, are shown in Fig. 4. It can be immediately noticed that, the larger Δ, the smaller the fractal dimension Δ_σ of the contact domain (i.e., the larger its *lacunarity*).

If the area of true contact is plotted vs the applied load, [4] at a fixed resolution s (Fig. 5(a)), a nearly linear behaviour is observed ($A_r \sim P$) for all values of the fractal dimension. It is remarkable to notice here that disorder, which is usually associated with non-linearity and chaos, yields in this case linear behaviour. This is in agreement with the early observations by Archard [12], and Greenwood and Williamson [13] and with many experimental results in the literature. Note, however, that Majumdar and Tien [17] found a non-linear relation ($A_r \sim P^\alpha$, $1.0 \leqslant \alpha \leqslant 1.33$), based on their model of elastic–plastic contact between fractal surfaces. The effective interface closure can be approximated by subtracting, from the total displacement δ_z, the part due to the linear elasticity of the half-spaces. This bulk contribution depends only on P and can be evaluated by considering uniform pressure on the nominal loaded area. In this way, the non-linearity, due to the interface roughness, can be put into evidence. By fitting the data with a hyperbola, the asymptotes of the diagram can be estimated, which correspond to the complete closure of the joints. It can be noticed that, as the fractal dimension of the surface increases, the extension of the closing stage increases, together with the interface compliance (Fig. 5(b)).

Another fundamental aspect to be highlighted is the dimensional evolution of the contact domain S, which is initially very rarefied and progressively increases its topological density at larger loads. As the

[4] Note that the units of forces and lengths in Figs. 5, 6, 10–13, are arbitrary, since we are interested only in the qualitative behaviour of mathematical surfaces.

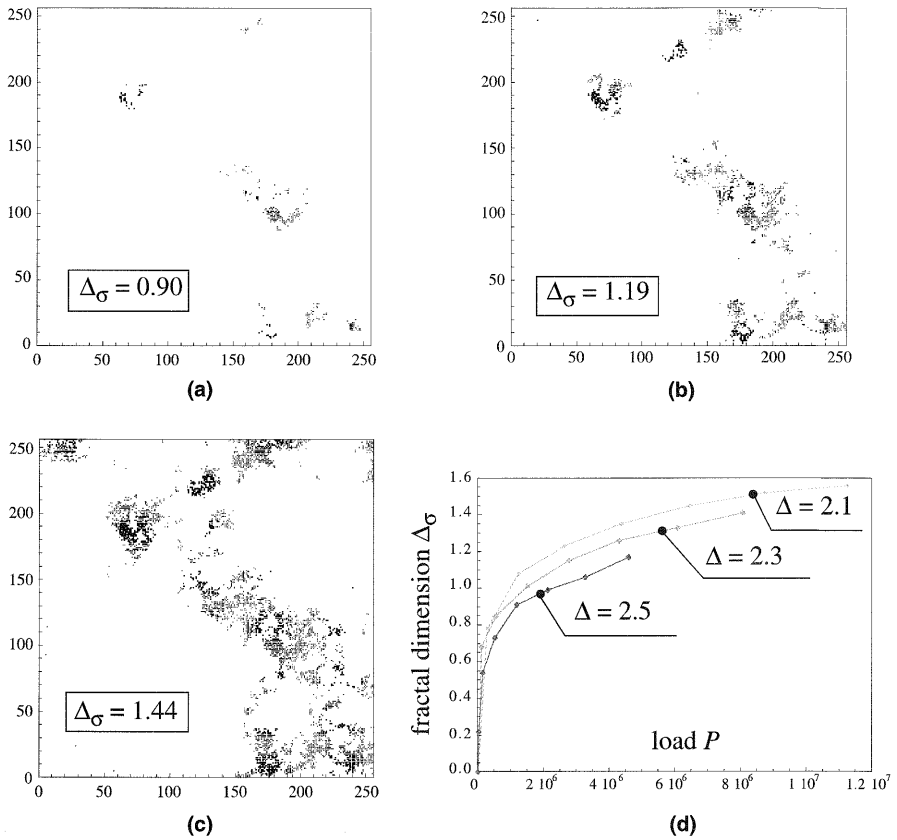

Fig. 6. Three contact domains (a)–(c) at different loads for the same mathematical surface ($\Delta = 2.3$, $s = 1/256$), and evolution of the fractal dimension with load (d).

apparent pressure σ_0 between the half-spaces increases, the classical theories yield the increase of the number of contact spots, that is, the increase of the real contact area A_r. However, since the euclidean measure of A_r is experimentally depending on the measurement precision (or on the numerical discretization), the classical elastic contact theories do not have unique predictive capabilities. By using the box-counting method, it can be shown that, as the normal load P increases, the fractal dimension Δ_σ starts from a value close to 0.0 (corresponding to pointwise non-structured contact), and subsequently takes values larger than unity as soon as linear contact structures and rarefied contact *islands* are formed (Fig. 6). The total saturation of the contact domain S (or, at least, of some *islands*) would imply $\Delta_\sigma = 2.0$. This value, in real materials, can be attained only under very high normal loads, implying the extended plasticization of the material. In this limit case, the euclidean description would be consistent and the physical quantities would retain their usual integer dimensions. In the limit of $\Delta_\sigma \to 2.0$, size-effects would disappear, and a scale-independent friction coefficient could be defined. Ciavarella et al. [19] have shown, for the particular case of a two-dimensional fractal profile (Weierstrass graph), that in linear elasticity the contact domain remains lacunar for any value of the applied load. However, in contrast with the numerical results, they found a constant fractal dimension of the contact domain. It may be argued that this discrepancy is due to the lower length cut-off of the numerical calculations.

3.4. Mechanical response of natural rock interfaces

A cylindrical specimen of initially uncracked fine-grained sandstone has been fractured at midspan in three-point bending (Fig. 7). The diameter of the specimen was equal to 50 mm. After breaking the specimen, the fracture surface at one side was digitised by means of a laser profilometer with a fixed resolution of 100 μm. It is believed that further refinements, in the case of this rock, would not alter

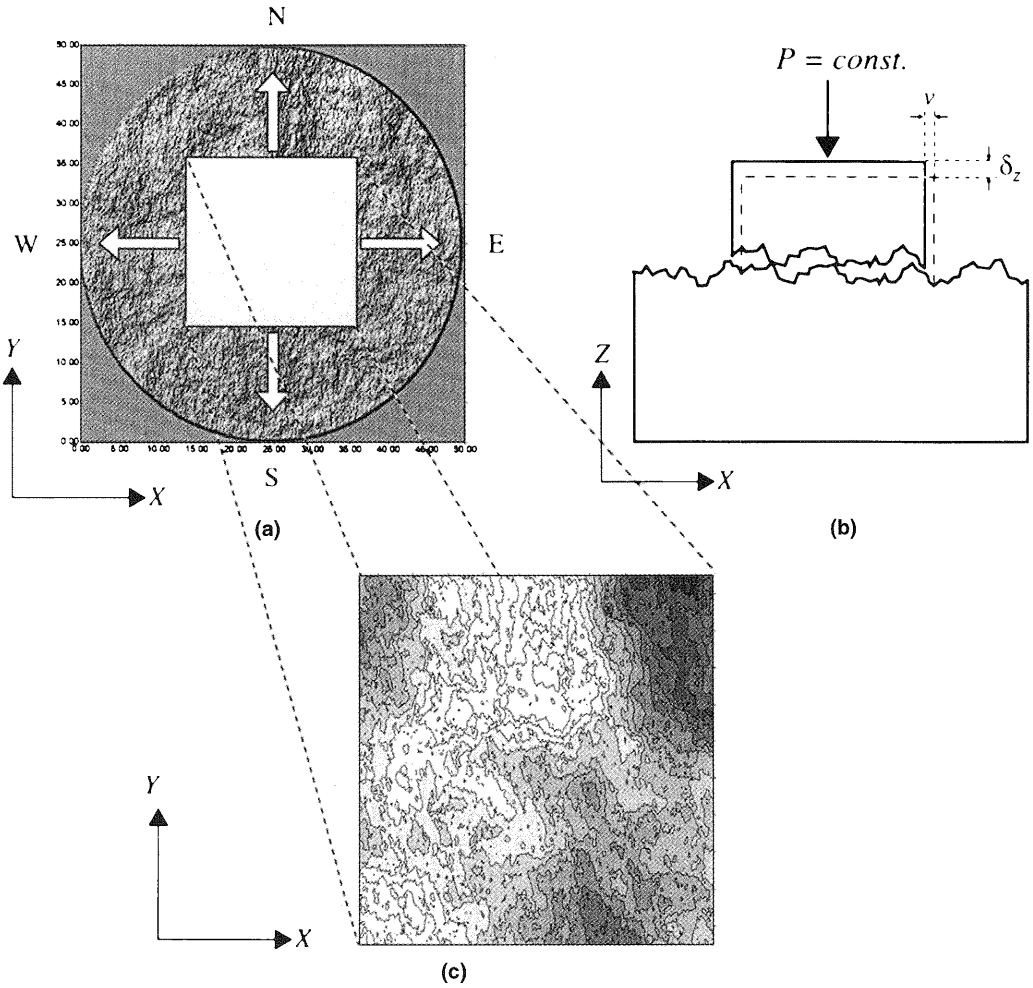

Fig. 7. Scheme of the numerical simulation on the rock joint: normal displacement δ_z, imposed horizontal shifting v, and composite topography (c) obtained for $v = 10$ mm.

significantly the numerical simulation of contact, at least in the desired mesoscopic scale range. Due to the remarkable homogeneity of the considered surface, the scanned area (1962 mm^2) can be considered as a representative surface for the contact behaviour of this rock joint. The calculated fractal dimension Δ of the surface is equal to 2.21. Only one side of the fracture was digitized, because the hypothesis of perfectly corresponding surfaces at the opposite sides of the fracture is implicitly assumed in the following. Therefore, in the case of fracture surfaces, simulations must be performed after applying a relative shift v to the opposing faces. This gives rise to a composite topography Δh different from zero (Fig. 7(c)).

If the area of true contact is plotted vs the applied load, a nearly linear behaviour ($A_r \sim P$) is observed, as in the case of the mathematical surfaces (Fig. 5(a)), for any value of the tangential shift. In Fig. 8(a), the effective closure curves obtained, for the rock interface, in correspondence of five different values of the relative offset v (west direction), are shown. By fitting the data with a hyperbolic function, the asymptotes of the curves can be estimated, which correspond to the complete closure of the joints. It can be noticed that, as the initial offset v increases, the extension of the closing stage increases, together with the interface compliance. This corresponds to the increase of the fractal dimension of the *composite topography*. However, this is true only for the very initial stages of sliding. After a certain shifting, the curves overlap and the joint deformability becomes constant. On the other hand, when v becomes very large ($v \approx 10$ mm), the joint compliance increases again because no more correlations are present between the opposite pushing surfaces (see the last contact domain in Fig. 8(d)). Finally, by comparing samples of different sizes, it was

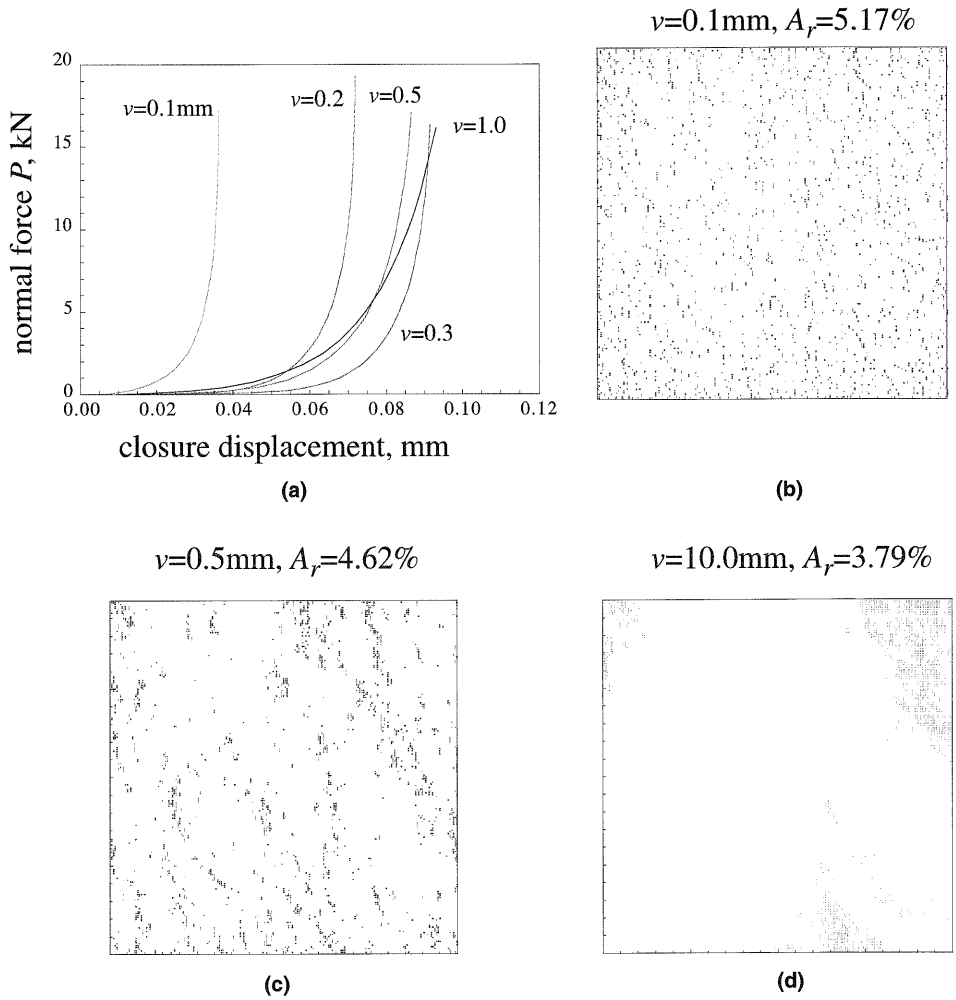

Fig. 8. Crack closure laws of the rock interface (at fixed resolution) for different horizontal shifting (a). Calculated contact domains (at fixed normal load $P = 10000$ N) for three different values of the shift v (b)–(d).

noticed that the larger the samples, the larger the closure deformability, independently of the relative shear displacement. This again is due to lacunarity of the contact domain, i.e., to the higher probability of finding larger voids in larger specimens' domains.

4. Discrete tangential contact of rough surfaces

4.1. General statement of the problem

It is known that, in a general contact in *gross* or *full*-sliding, the condition to obtain pure relative translation is the application of a tangential force through the *centroid* of the normal micro-forces G_P, i.e., the point of application of the normal force. [5] However, the condition for full-sliding cannot be reached, other than through an increase of the tangential force starting from zero. Now, when a tangential load is applied to a general contact between elastic bodies, a complex frictional shear traction distribution $\mathbf{q}(x, y)$ arises to equilibrate the applied load. The contact area is divided into regions of micro-slip and regions of

[5] This is actually true, a rigori, only in the absence of Poisson's effects.

adhesion, according to Coulomb's law, and the position of the centroid of shear forces is not necessarily coincident with G_P.

Problems in the tangentially loaded regime invariably reduce to finding the correct size and location of stick and slip areas, S_{stick}, S_{slip}, as well as the position of the *centroid of shear*, G_Q, and the the *direction* of slip, which in general must be postulated and checked a posteriori. The conditions in terms of equalities and inequalities are given by Eqs. (7a) and (7b) and by the classical Coulomb friction law, which can be summarized by writing:

$$|\mathbf{q}(x,y,t)| < fp(x,y,t) \quad (x,y) \in S_{\text{stick}}, \tag{14a}$$

$$|\mathbf{q}(x,y,t)| = -fp(x,y,t)\frac{\partial}{\partial t}\frac{\mathbf{g}_t(x,y,t)}{|\mathbf{g}_t(x,y,t)|} \quad (x,y) \in S_{\text{slip}}, \tag{14b}$$

where f is the friction coefficient. Note that the vectorial notation is necessary because, in general, $\mathbf{q}(x,y)$ has two components, and a fictitious time variable t is introduced to impose shear to be aligned with the direction of relative change in the direction of slip. [6] Finally, $\mathbf{g}_t = g_x\boldsymbol{e}_x + g_y\boldsymbol{e}_y$ is the *relative* tangential displacement. The solution of the problem is, in general, incremental [2,20]. On applying a monotonically increasing tangential load in direction x, there will in general be stick and slip zones. The shear tractions are strictly related to the limiting value of Coulomb friction (see below). The other two (discretized) integral equations defining the problem both relate to elastic displacements of points parallel to the surface, one in the direction of the tangential force, and the other perpendicular to it. They are, putting $\beta = 0$ in Eqs. (2) and (3)

$$u_{xi} = \frac{A}{2\pi}\sum_{j}^{N}\left[\frac{q_{xj}}{r_{ij}} + \gamma\left(\frac{(x_j - x_i)^2}{r_{ij}^3}q_{xj} - \frac{(x_j - x_i)(y_j - y_i)}{r_{ij}^3}q_{yj}\right)\right], \tag{15}$$

$$u_{yi} = \frac{A}{2\pi}\sum_{j}^{N}\left[\frac{q_{yj}}{r_{ij}} + \gamma\left(\frac{(y_j - y_i)^2}{r_{ij}^3}q_{yj} - \frac{(x_j - x_i)(y_j - y_i)}{r_{ij}^3}q_{xj}\right)\right] \tag{16}$$

for $(x_i, y_i) \in S$. It is clear that, even though we are considering the $\beta = 0$ case, there is a second coupling, due to γ, between the distributions of shear tractions themselves. Indeed, this system of coupled equations gives a solution $[q_x(x_i,y_i), q_y(x_i,y_i), (x_i,y_i) \in S]$ for any couple of assigned functions $[u_x(x_i,y_i), u_y(x_i,y_i)]$ in the contact domain S. Therefore, in the general case, even if we impose, say, $u_y(x_i,y_i) = 0$, due to the coupling it does not follow that $q_y(x_i,y_i) = 0$. Also, again due to the coupling, there is no analogy between the integral equation for the normal displacements and the tangential correspondents.

Therefore, in order to avoid coupling, and obtain an equation similar to Eq. (6), let us consider the case that the composite Poisson ratio of the bodies is zero, [7] $\gamma = 0$: in this case, the equations in tangential direction simplify to

$$u_{xi} = \frac{A}{2\pi}\sum_{j}^{N}\left[\frac{q_{xj}}{r_{ij}}\right], \tag{17}$$

$$u_{yi} = \frac{A}{2\pi}\sum_{j}^{N}\left[\frac{q_{yj}}{r_{ij}}\right], \tag{18}$$

which are two independent problems, each one analogous to a normal contact problem. The total shear forces are

$$Q_x = \sum_{j}^{N} q_{xj}, \quad Q_y = \sum_{j}^{N} q_{yj}. \tag{19}$$

[6] The condition written is valid under monotonic tangential loading.

[7] For materials having non-negative Poisson's ratio, this is only possible if both $\nu_1 = \nu_2 = 0$.

The condition we look for is the *pure relative translation*. Therefore, we seek here for conditions under which a simple solution (i.e., with only one component of shear traction distribution) for the pure relative translation problem is possible. Let us denote with x the direction of the resultant force, i.e., $Q_y = 0$: it is clear that we do not know a priori whether this is also the direction of the relative translation. However, as the shear tractions in the two bodies are equal and opposite for Newton's third law, the tangential displacement of the particles of one surface must be constant within the stick zone, and equal to the imposed relative rigid translation (δ_x, δ_y)

$$u_x(x_i, y_i) = \delta_x, \quad u_y(x_i, y_i) = \delta_y, \quad (x_i, y_i) \in S_{\text{stick}}, \tag{20}$$

where δ_y is expected to be zero under symmetry conditions. Moreover, Coulomb's law applies (Eqs. (14a) and (14b)), and the above equations provide the framework for solving the problem.

4.2. Solution of the problem by the discretized Cattaneo partial-slip method

Since in the normal loading phase there was no tendency for surface particles to slip, the initial stick zone envelopes the entire contact. A monotonically increasing tangential remote relative displacement will therefore give rise to a *receding* problem, according to Dundurs' classification [29], and therefore there is no need to follow the entire loading path, and we can solve directly for any particular value of δ_x.

In the classical continuous problem, it is usually assumed that, since the traction would be infinite at the boundary of the adhesion area, a part of the contact area must start sliding and the regime of partial-slip takes place. The analogy in [6,30] is sufficient to validate the assumption that full stick implies a singular distribution of shear traction, that cannot be sustained by a *finite* friction coefficient. Therefore, the mathematical problem of full stick is practically not very meaningful in this context, unless we consider the case where the bodies are welded together, i.e., we have an external crack problem with the singularity giving a stress intensity factor [31]. Although dealing with a discrete contact problem, we follow the same argument of the continuous case. Following [3,4], we assume a tangential traction distribution given by the sum of two components, a full-sliding term and a *correction*, that is

$$q_{xj} = fp_j - q^*_{xj}, \tag{21}$$

where $q^*_{xj} = 0$ in the region of slip, i.e., for $(x_j, y_j) \in S_{\text{slip}}$, whereas it is at yet undetermined in the stick region. With the previous hypotheses, Eq. (18) in the y-direction is identically satisfied, whereas, writing again Eq. (17) for the elastic displacements in the tangential direction x, we get

$$u_{xi} = \frac{A}{2\pi} \sum_j^N \left[\frac{q_{xj}}{r_{ij}} \right] = \frac{A}{2\pi} \sum_j^N \left[\frac{fp_j}{r_{ij}} \right] - \frac{A}{2\pi} \sum_j^{N^*} \left[\frac{q^*_{xj}}{r_{ij}} \right] = fu_{zi} - \frac{A}{2\pi} \sum_j^{N^*} \left[\frac{q^*_{xj}}{r_{ij}} \right], \tag{22}$$

where we have used Eq. (21) and we have indicated with N^* the number of points in the stick region. Rearranging the last equation, we have

$$u_{zi} - \frac{u_{xi}}{f} = \frac{A}{2\pi} \sum_j^{N^*} \left[\frac{(q^*_{xj}/f)}{r_{ij}} \right] = \frac{A}{2\pi} \sum_j^{N^*} \left[\frac{p^*_j}{r_{ij}} \right], \tag{23}$$

which can be recognized as being of the same kind as the original Eq. (6) involving the normal pressures, for a lower value of the vertical rigid body displacement, giving the resulting 'contact' area (i.e., the stick area) to be a subregion of the actual contact area. Note that the rotation is the one fixed by the actual normal contact problem, i.e., by Eqs. (7a) and (7b).

Eqs. (21)–(23) can be regarded as the elastic version of Coulomb's law, the tangential forces being the difference between the actual normal force and the normal force for a smaller contact area, multiplied by the coefficient of friction [7]. Eq. (23) represents the discrete version of the theorem proved in [6]. Since p_j is always greater than p^*_j, their difference is always positive and the inequalities always hold. Several

elementary properties can be deduced: (i) flat regions are either entirely in full stick or in full-slip conditions, as in unloading they either stay in contact, or lose contact simultaneously. In the limiting case of an entirely flat contact, the behaviour is full stick/full-slip; (ii) the points that lose contact first in the normal unloading, with the fixed rotation of the actual normal contact problem, are the first to slip when the tangential force is imposed; (iii) the tangential approach δ_x can be calculated from the two normal approaches of the normal contact problems, as

$$\delta_x = f(\delta_z - \delta_z^*); \tag{24}$$

(iv) the shape of the stick zone is the one that maximizes the corrective load for a given corrective normal approach, therefore the shape of the slip area is the one that minimize the full-sliding component; (v) if the indenter profile is symmetrical and self-similar, the stick zone is similar to the initial shape, and the corrective solution is always of the same functional form of the normal pressure in the contact area; (vi) finally, it has been shown in the previous sections that, for rough surfaces, the real contact area is nearly proportional to the normal force [12,13,18]. It follows that the slip area must be proportional to the tangential force because it is the difference between two contact areas, both proportional to the pertinent normal force.

5. Numerical simulation of the partial-slip process

5.1. Stick-slip domains and position of the centroid of shear

By applying the theory outlined in the previous section, it is possible to investigate, step by step, the partial-slip process occurring at rough interfaces. As already pointed out before, in the numerical model we have to substitute point forces p, q_x, with the resultants $\bar{p}$, $\bar{q}_x$, acting upon the finite-size flat punch representing the asperity cap at the given resolution. It must be kept in mind, however, that a true partial-slip regime, in the case of rough surfaces, can take place only if the relative sliding displacements are smaller than the average size of the asperities. In the numerical simulations, this implies that the slip displacements must be smaller than the adopted resolution. In this case, the interlocking effects come into play only when full-slip occurs, and the dilatancy behaviour becomes predominant.

In Fig. 9 the contact domain for the brownian surface with $\Delta = 2.3$, is observed, at a given value of the normal load P, by increasing the value of the total shear force Q. The stick points are black, while the points where slip occurs are grey. It can be observed that, as in the Hertzian case, the slip areas proceed inwards from the edges of the contact area. In fact, partial-slip takes place in the external parts of the

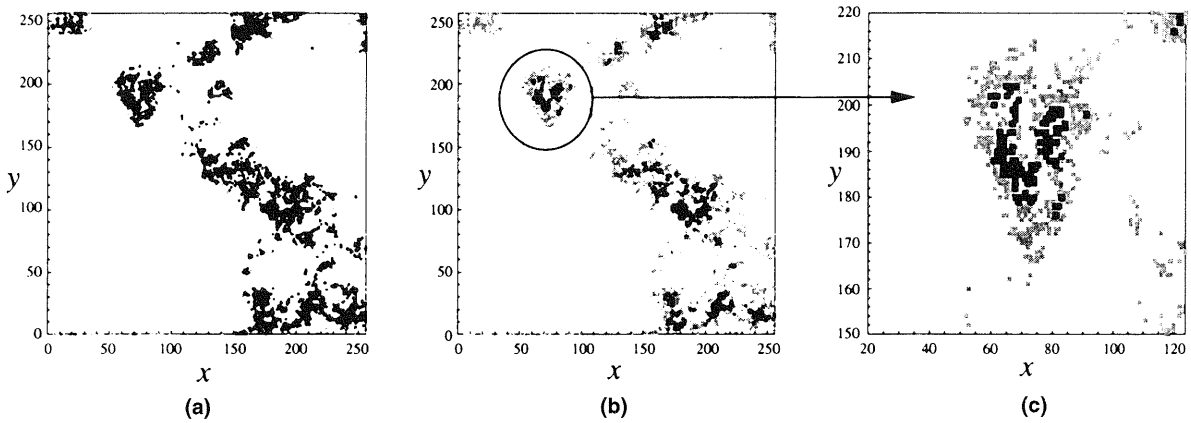

Fig. 9. Extent of the stick (black) and slip (grey) areas of contact for two increasing values of the applied shear force Q (mathematical surface, $\Delta = 2.3$) (a) and (b). Enlargement of a zone in the second contact domain (c).

contact clusters, where the normal forces are smaller than in the inner parts. This, of course, depends on the distribution of peaks and valleys in the composite topography of the surfaces in contact. The same behaviour has been observed for the contact domains generated in natural interfaces.

In the case of the rock interface, it is interesting to plot the measures of the stick and slip area as functions of the applied shear force (Fig. 10(a)). It can be seen that the behaviour is linear, as one could expect by considering that the tangential solution is obtained by means of an analogy with normal solutions. More significantly, plotting the amount of shear force carried respectively by the stick (Q_{stick}) and by the slip (Q_{slip}) domains, one notes that, initially, both quantities increase with the total shear force Q as the slip area monotonically grows, whereas, after a while, Q_{stick} starts to decrease (Fig. 10(b)). The behaviour, in this case, is non-linear.

In correspondence of any value of Q, the position of the centroid of the shear forces G_Q can be computed for the stick domain as well as for the slip one. Note that the centroid $G_{Q(\text{slip})}$ in the slip part coincides with the centroid $G_{P(\text{slip})}$ of the normal pressures acting in the same domain, due to the linear proportionality of Coulomb's law. Instead, the centroid $G_{Q(\text{stick})}$ of the shear forces within the stick part is not coincident with $G_{P(\text{stick})}$, due to the correction term of the Cattaneo solution. Therefore, the horizontal position of the global centroid of shear G_Q is given by

$$x_{G_Q} = \frac{x_{G_{Q(\text{slip})}} Q_{\text{slip}} + x_{G_{Q(\text{stick})}} Q_{\text{stick}}}{Q_{\text{slip}} + Q_{\text{stick}}}, \tag{25a}$$

$$y_{G_Q} = \frac{y_{G_{Q(\text{slip})}} Q_{\text{slip}} + y_{G_{Q(\text{stick})}} Q_{\text{stick}}}{Q_{\text{slip}} + Q_{\text{stick}}}, \tag{25b}$$

It is interesting, for instance, to follow the evolution of G_Q as the total shear increases from zero to the full-sliding value ($Q_{\max} = fP$). Note that, due to the properties of the Cattaneo solution, the reverse path can be interpreted as the evolution of the centroid G_P when the normal force increases from zero to its final value $P_{\max}$. In Fig. 11, relative to a rock interface (a) and to a concrete interface (b), the centroid G_Q tends to move away from the geometrical centroid as the total shear force increases. This implies that the external shear force Q should be continuously adapted to the growing eccentricity, otherwise torsional effects come into play. If the reverse path is considered, (i.e., by increasing P with $Q = 0$), G_P tends to approach the geometric centroid of the interfaces, which plays the role of an *attractor*. This result implies that we are dealing with statistical homogeneous interfaces.

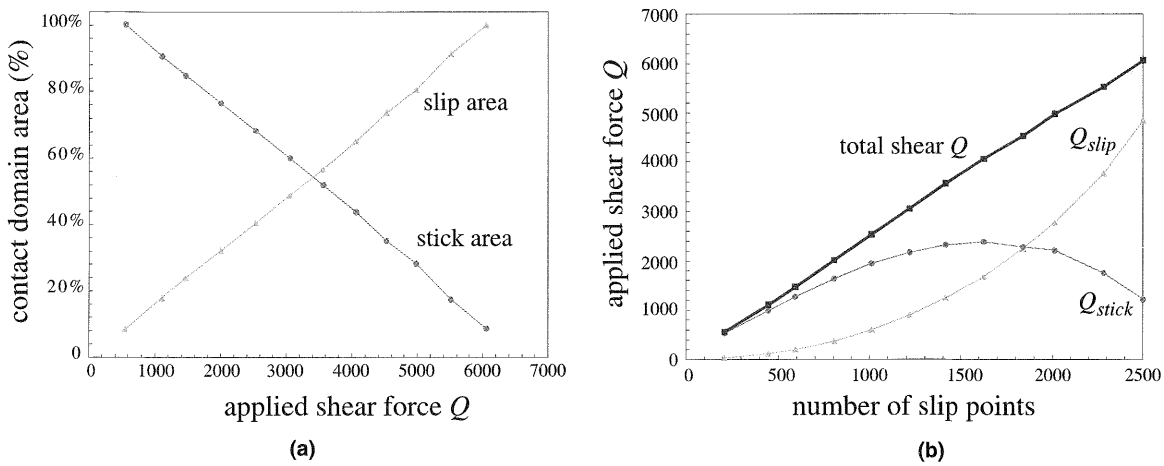

Fig. 10. Linear variation of the extent to stick and slip area with the applied shear force (a). Non-linear variation of the fractions of shear force carried respectively by the stick (Q_{stick}) and by the slip (Q_{slip}) domains (b).

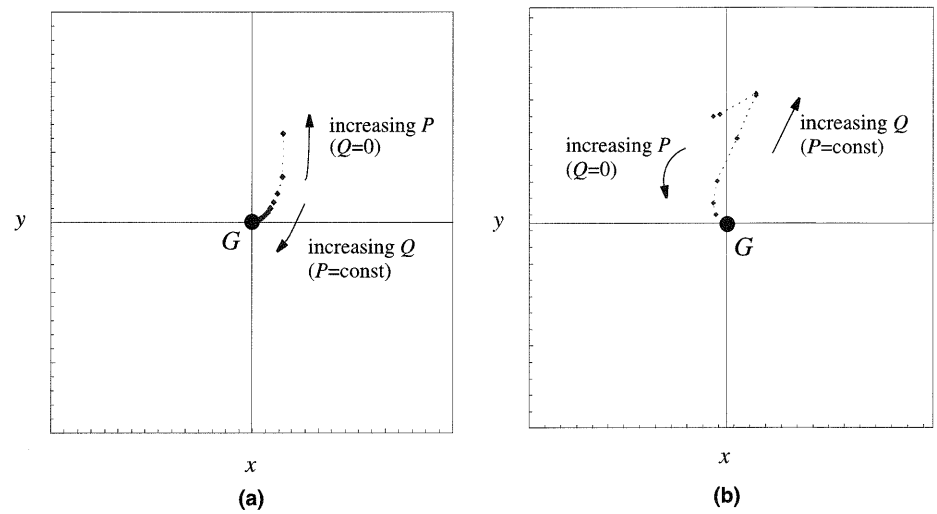

Fig. 11. Calculated evolution of the position of the centroid of shear G_Q in a rock interface (a) and a concrete fracture (b).

5.2. Energy dissipation during partial-slip

The elastic analogy by Cattaneo allows one to calculate the distribution of energy dissipation in the micro-slip zones. Assuming, for instance, sliding along the X-axis, the specific energy E_f dissipated by friction in correspondence of any slipping asperity can be easily obtained as

$$E_f(x,y) = \bar{q}_x(x,y)g_x(x,y) = f\bar{p}(x,y)g_x(x,y), \tag{26}$$

where $g_x(x,y)$ represents the relative sliding displacement in the micro-slip zones to be computed by means of the Cattaneo solution. It can be argued that most of this energy results in heat production. However, this solution implies that the slipping asperity is free to slide of the calculated quantity u_x. Analysis of the dilatancy behaviour, on the other hand, shows that this is not always possible, in the sense that asperities interlocking may occur before the complete displacement has developed. This imposes a strong limitation to the Cattaneo solution or, better, to the scale at which it can be considered valid also for displacements.

When the condition of incipient full-sliding is reached, the correction terms vanish and Eq. (22) yields: $u_x(x,y) = f\Delta h(x,y)$, where $\Delta h(x,y)$ is the original distance between two corresponding points at the interface. Therefore, the energy necessary to attain the condition of incipient full-sliding can be obtained by summing over the entire contact domain S, as

$$E_f^{\text{tot}} = \sum_S f^2\bar{p}(x,y)\Delta h(x,y). \tag{27}$$

Calculation of this quantity is usually performed by a Winkler approach (i.e., assuming the asperities to be independent elastic springs). In that model, $\bar{p}(x,y) \sim \Delta h(x,y)$, and also the area of the contact domain has a trivial dependence on the normal load. Instead, in our contact model, all the interactions among the asperities are involved in the determination of the contact domain. In Fig. 12, the relation between dissipated energy E_f and normal load P is plotted for three different fractal surfaces. As the fractal dimension increases, the dissipated energy for a given value of normal load increases too. Moreover, the dependence of E_f on P is clearly non-linear.

One has to remind that, of course, displacements become undetermined at full-sliding. The energy above, however, is extremely meaningful, for instance in presence of fretting fatigue, where Eq. (27) allows to compute the energy dissipated during cyclic load histories. Another potential field of application could be seismology, where the analysis of the precursors of a major fault event is of crucial importance for earthquake predictions.

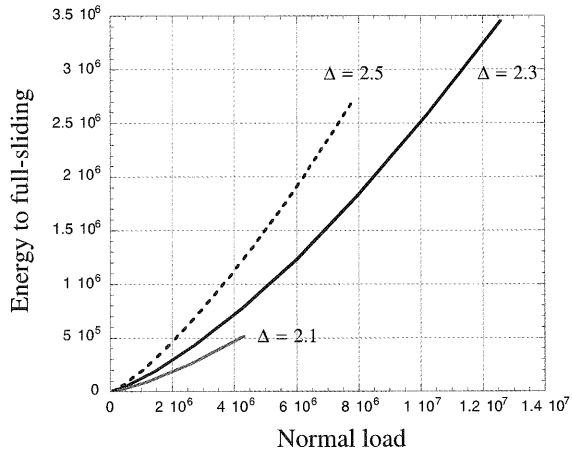

Fig. 12. Non-linear dependence of the dissipated energy E_f on the normal load P (mathematical surfaces). The dissipated energy (at a given value of P) increases with the fractal dimension of the interface.

6. Multifractal distribution of the contact pressure fields

The ability of the numerical model to calculate normal and tangential forces at all the contact points permits to highlight some hidden features of the problem. The distributions of the contact normal forces in the synthetical interfaces as well as in the rock joint have been investigated, at a fixed value of the resolution.

In the case of the mathematical interfaces, the statistical distributions of the forces $\bar{p}_i$ exerted at the contact points, under the same external load (i.e., under the same nominal pressure) are reported in Fig. 13. It can be concluded that the distribution of local micro-forces tends to become more uniform as the fractal dimension increases. The histograms also show that only a few points undergo very high stresses, especially for the lower fractal dimensions. This supports the early observation reported in [13], i.e., that plastic deformations should not add significant new features to the contact model, at least in a wide loading range. It can be also shown that the population of the $\bar{p}_i$ obeys a semi-log distribution, whereas the $\bar{p}_i^2$ distribution fulfills a power-law, i.e., $\log(N) \sim \beta \log(\bar{p}_i^2)$, where N is the number of asperities bearing a pressure equal to $\bar{p}_i$. If the hypothesis is made that the elastic energy released by slipping asperities is proportional to the square of the pressure ($W_i \sim \bar{p}_i^2$), the distribution of energy releases follows a power-law. Note that this corresponds to the well-known recurrence power-law of seismic events [32].

A related aspect is the spatial distribution of micro-forces, which shows multifractal characteristics. The mathematical description of this kind of distributions can exploit the concept of *multifractal measures* [14]. In this context, the term 'multifractal' implies that the contact domain S is made out of infinite fractal subsets, each one with its own fractal dimension and thus with its own scaling properties. The pertinent kind of singularity of the micro-forces distribution can be associated to each of these subsets. If $\bar{p}[B(x,y,r)]$ is the resultant of the micro-forces acting in the circle B, centered at point (x,y), with radius a, the local dimension of the measure $\bar{p}$ in (x,y) is $\alpha(F,x,y)$ if

$$\lim_{r\to 0} \frac{\log \bar{p}[B(x,y,r)]}{\log r} = \alpha(F,x,y). \tag{28}$$

Under the assumption of sufficiently small r, it is therefore possible to write

$$\bar{p}[B(x,y,r)] \sim r^{\alpha(F,x,y)}. \tag{29}$$

If point P were placed in a classical (euclidean) contact area (locally smooth contact, $\Delta_\sigma = 2$), one would obtain

$$\bar{p}[B(x,y,r)] \sim r^2 \tag{30}$$

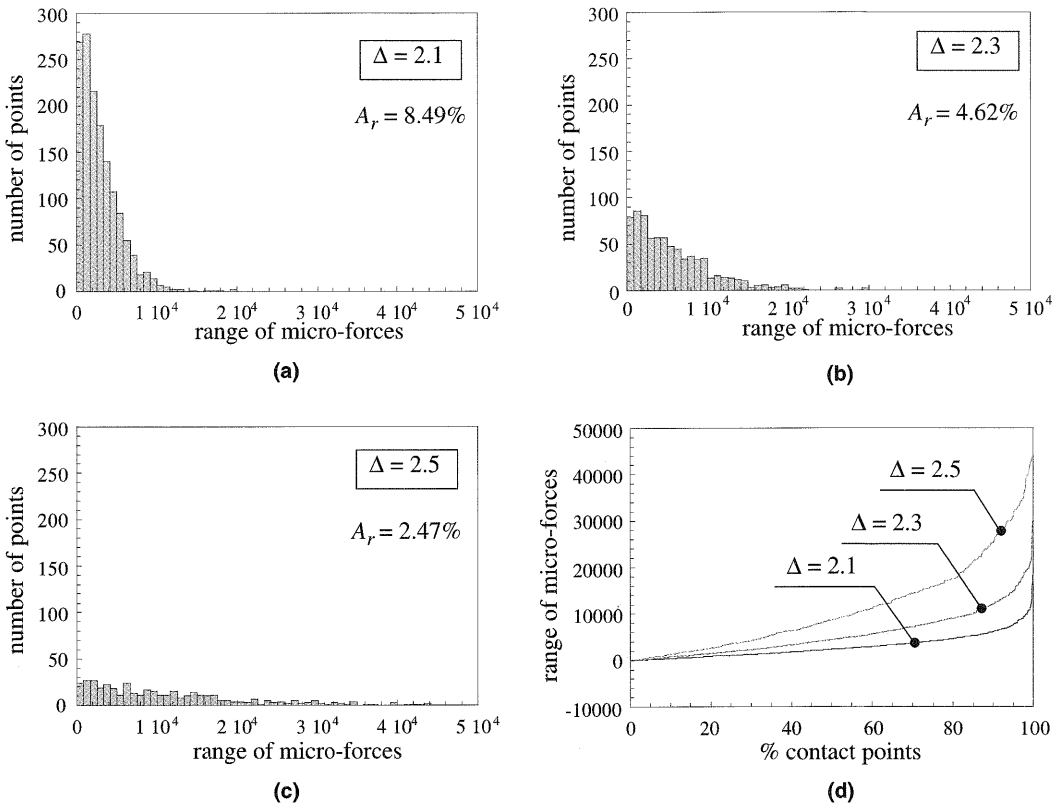

Fig. 13. Histograms (a)–(c) and cumulative distributions (d) of the local contact forces at the same external load P. Note that the total amount of contact points decreases as the fractal dimension of the surface increases.

and the pressures would correspond to the classical definition of Cauchy stress σ, with physical dimension $[F][L]^{-2}$. In the case $\alpha < 2$, the non-integer exponent α corresponds to the power of the local singularity of the micro-forces, and is named *Hölder exponent*. Although α depends on the considered position within the contact domain S, there are usually many subsets characterized by the same exponent α. If the micro-forces were uniformly distributed over S, each subset would be characterized by the same value $\alpha = \Delta$. However, reality is more complex. A particular subset S_α of the contact domain can be defined for each value of α, including all the points where the singularity of the contact force $\bar{p}$ exhibits an exponent equal to α. To describe the singularities and their spatial distribution, the properties of the S_α subsets need to be studied. For this purpose, the most expressive mathematical tool is represented by the *spectrum of dimensions*, which relates, to each local exponent α, the fractal dimension $f(\alpha)$ of the subsets S_α.

Put into practice, the contact domain S is divided into N boxes, corresponding to the discretization adopted for the elastic simulations, and the number of boxes $n(s,\alpha)\,d\alpha$, where the local fractal dimension is comprised between α and $\alpha + d\alpha$, is computed. Thereby one gets

$$f(\alpha) = \lim_{s\to 0} \frac{\log n(s,\alpha)}{-\log s}. \tag{31}$$

The function $f(\alpha)$ is called *spectrum of the exponents*, and is generally a continuous curve with a maximum equal to the fractal dimension Δ_σ of the support (i.e., of the contact domain).

In the case of the rock joint, some multifractal spectra, computed for different values of the normal load P, or for different values of the relative horizontal shift v, are shown in Fig. 14. Note that the micro-forces distribution depends on the relative shift between the crack faces, because the composite topography changes with v. In particular, the width of the spectrum is reduced as the offset increases, and the maxima progressively decrease (Fig. 14(a)). It is also interesting to note that the distributions depend on the normal load (Fig. 14(b)). As P increases, in fact, the maximum value of the spectrum ($\max f(\alpha)$) becomes higher,

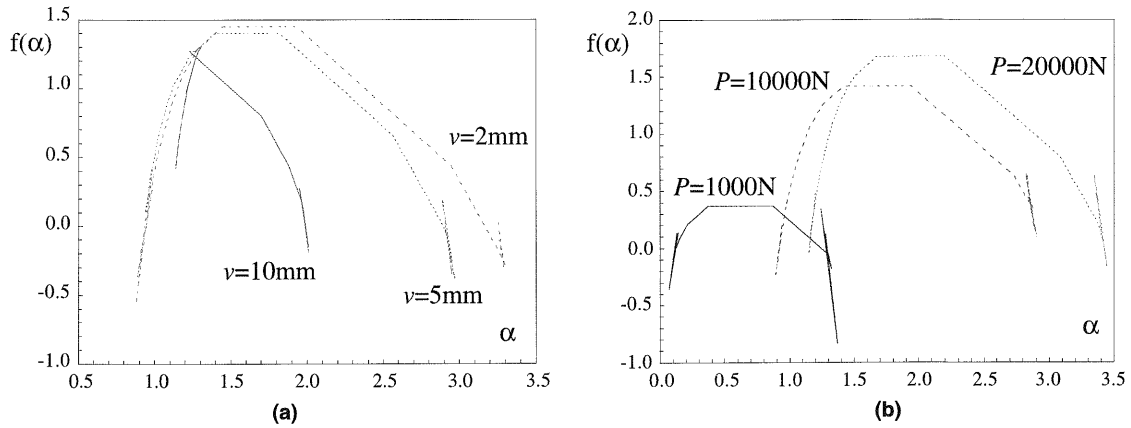

Fig. 14. Multifractal analysis of the distribution of contact micro-forces at the rock interface. Calculated spectra, for P = constant, by varying the horizontal shift v (a). Calculated spectra, for v = constant, by increasing P (b).

according to the dimensional evolution of the contact domain. The width of the spectrum increases too, because the range of micro-forces is progressively enlarged (new asperities come into contact, while the pressure grows in the previous ones).

7. Conclusions: capabilities and limits of the model

In this paper, the Cattaneo–Mindlin theory of frictional contact has been extended to elastic half-spaces in contact through disordered self-affine interfaces. The discretized formulation of the Cattaneo theorem is also provided, and represents the basis of the proposed numerical model. Mathematically generated surfaces with different roughness, and experimentally digitised ones have been analysed. The capability of fractal geometry to describe real disordered interfaces permits to capture some peculiar aspects of contact mechanics.

By means of the numerical method, the evolution of the contact domain under monotonic loading has been investigated. We have proven the correspondence to the experimental findings reported in [12,13]. It has been shown that, for constant normal pressure and increasing shear force, the extent of the stick area decreases in the same way as the contact area develops with increasing pressure. The slip area is found to be proportional to the tangential force, as predicted by Cattaneo theory. Correspondingly, the size of the stick zones decreases as the tangential force increases. Self-affinity of the interfaces results in the lacunarity of the contact domains, whose fractal dimension, smaller than 2.0, appears to increase with the nominal pressure. At a sufficient level of discretization, contact pressures show multifractal distributions, i.e., a spectrum of dimensions is necessary to describe all the moments of their distribution. The spectra change during the loading history, according to the topologic evolution of the contact domain.

Although many basic features of the tangential problem are captured by the above method, a limitation is represented by the purely linear elastic behaviour and by the assumption of constant friction coefficient. In particular, the last assumption eliminates the possibility of modeling the instabilities often emerging in sliding contact. Explicit energy exchange among the slipping asperities should be considered. That is, if an asperity attains its limit tangential force, it slips and some elastic energy is released. This energy is partially dissipated at the interface and partially transmitted (by a stress wave) to the surrounding asperities. Similar arguments were already exploited in 1967 by Burridge and Knopoff in their famous model for seismicity [33], where, however, the contribution of disorder was not taken into account. Another way to implement the mutual interactions could be that of considering a *kinetic* local friction coefficient f_k smaller than the *static* one. In this way, once the asperity attains its limit tangential force, its coefficient drops and thus a certain amount of shear force ($\Delta q_i = (f - f_k)p_i$) must be transferred to the surrounding elements under constant total shear. In both cases, an increase of the tangential forces in the neighbourhood of the slipped

asperity should be taken into account. The transition from stable shear loading (partial-slip, macroscopically firm body) to instability (full-slip) is critical in the sense that collapse can be sudden and occur much before than all the asperities reach their local friction limit. This is provided by a cooperative phenomenon generated by local slip events, due to the aforementioned energy releases. The first events are smoothly absorbed by the stick domain, but at a certain critical point the local slips could activate a cascade process leading to full-slip. An incremental load history becomes necessary to model these features.

Regardless of its limitations, the Cattaneo–Mindlin solution can be successfully exploited in the cases of cyclic tangential loadings below the full-slip condition. For instance, this is the case of fretting fatigue, which is nowadays recognized as a crucial topic for the assessment of safety and residual life of mechanical components.

References

[1] H. Hertz, Über die Berührung fester elastischer Körper, J. Reine Angew. Math. 92 (1882) 156–171.
[2] K.L. Johnson, Contact Mechanics, Cambridge University Press, Cambridge, 1985.
[3] C. Cattaneo, Sul contatto di due corpi elastici: distribuzione locale degli sforzi, Rendiconti dell'Accademia Nazionale dei Lincei 27 (1938) 342–348, 434–436, 474–478.
[4] R.D. Mindlin, Compliance of elastic bodies in contact, J. Appl. Mech. 16 (1949) 259–268.
[5] R.D. Mindlin, H. Deresiewicz, Elastic spheres in contact under varying oblique forces, J. Appl. Mech. 20 (1953) 327–344.
[6] M. Ciavarella, The generalized Cattaneo partial slip plane contact problem. I-Theory, II-Examples, Int. J. Solids Struct. 35 (1998) 2349–2378.
[7] J. Jager, A new principle in contact mechanics, J. Tribol. 120 (1998) 677–684.
[8] J.L. Lubkin, Torsion of elastic spheres in contact, J. Appl. Mech. 18 (1951) 183–187.
[9] M. Pacelli, Contatto con attrito tra due corpi elastici di forma qualunque: compressione e torsione, Ann. Scuola Norm. Sup. Pisa 10 (1956) 155–184.
[10] M. Hetenyi, P.H. McDonald, Contact stresses under combined pressure and twist, J. Appl. Mech. 25 (1958) 396–401.
[11] D.A. Hills, A. Sackfield, The stress field induced by a twisting sphere, J. Appl. Mech. 54 (1986) 8–14.
[12] J.F. Archard, Elastic deformation and the laws of friction, Proc. Roy. Soc. London A 243 (1957) 190–205.
[13] J.A. Greenwood, J.B.P. Williamson, Contact of nominally flat surfaces, Proc. Roy. Soc. London A 295 (1966) 300–319.
[14] J. Feder, Fractals, Plenum Press, New York, 1988.
[15] A. Majumdar, B. Bhushan, Role of fractal geometry in roughness characterization and contact mechanics of surfaces, J. Tribol. 112 (1990) 205–216.
[16] A. Carpinteri, B. Chiaia, S. Invernizzi, Three-dimensional fractal analysis of concrete fracture at the meso-level, Theoret. Appl. Fract. Mech. 31 (1999) 163–172.
[17] A. Majumdar, C.L. Tien, Fractal characterization and simulation of rough surfaces, Wear 136 (1990) 313–327.
[18] M. Borri-Brunetto, A. Carpinteri, B. Chiaia, Lacunarity of the contact domain between elastic bodies with rough boundaries, in: Probabilities and Materials. Tests, Models and Applications, NATO ASI Series 3, Kluwer Academic Publishers, Dordrecht, 1998, pp. 45–64.
[19] M. Ciavarella, G. Demelio, J.R. Barber, Y.H. Jang, Linear elastic contact of the Weierstrass profile, Proc. Roy. Soc. London A 456 (2000) 387–405.
[20] J.R. Barber, Elasticity, Kluwer Academic Publishers, Dordrecht, 1992.
[21] L.E. Goodman, Contact stress analysis of normally loaded rough spheres, J. Appl. Mech. 29 (1962) 515–522.
[22] P.D. Panagiotopoulos, A nonlinear programming approach to the unilateral contact- and friction-boundary value problem in the theory of elasticity, Ing. Arch. 44 (1975) 421–432.
[23] N. Kikuchi, J.T. Oden, Contact Problems in Elasticity: A Study of Variational Inequalities and Finite Element Methods, SIAM, Philadelphia, 1988.
[24] J.J. Kalker, Three-dimensional Elastic Bodies in Rolling Contact, Kluwer Academic Publishers, Dordrecht, 1990.
[25] A. Klarbring, Mathematical programming in contact problems, in: Computational Methods in Contact Mechanics, Computational Mechanics Publications, Southampton, 1993, pp. 233–263.
[26] Z.H. Zhong, Finite Element Procedures for Contact-Impact Problems, Oxford University Press, Oxford, 1993.
[27] A. Carpinteri, B. Chiaia, Power scaling laws and dimensional transitions in solid mechanics, Chaos, Solitons and Fractals 7 (1996) 1343–1364.
[28] A. Pinto da Cunha, Scale Effects in Rock Masses, Balkema, Rotterdam, 1993.
[29] J. Dundurs, Properties of elastic bodies in contact, in: Mechanics of Contact between Deformable Bodies, Delft University Press, Delft, 1975.
[30] M. Ciavarella, Tangential loading of general 3D contacts, J. Appl. Mech. 65 (1998) 998–1003.
[31] A.E. Giannakopoulos, T.C. Lindley, S. Suresh, Aspects of equivalence between contact mechanics and fracture mechanics: theoretical connections and a life-prediction methodology for fretting fatigue, Acta Mater. 46 (1998) 2955–2968.
[32] B. Gutenberg, C.F. Richter, Earthquake magnitude intensity, energy and acceleration, Bull. Seism. Soc. Am. 32 (1942) 1073–1075.
[33] R. Burridge, L. Knopoff, Model and theoretical seismicity, Bull. Seism. Soc. Am. 57 (1967) 341–371.